

Extreme downsizing in surfactant-free synthesis of spin-crossover nanoparticles in a microfluidic flow-focusing junction

Juan H. González-Estefan,^{ab} Mathieu Gonidec,^{ab*} Nathalie Daro,^{ab} Mathieu Marchivie,^{ab} and Guillaume Chastanet^{ab*}

^a CNRS, ICMCB, UMR 5026, F-33600 Pessac, France

^b Univ. Bordeaux, ICMCB, UMR 5026, F-33600 Pessac, France

Supporting Information

Experimental details:

Microfluidic chips:

We fabricated PDMS/PDMS chips (Silgard 184, 1:10 ratio of curing agent and base prepolymer) by conventional replica molding of silanized masters on 4" silicon wafers, obtained by photolithography through high-resolution transparent photomasks (Selba) using a UV-KUB 2 exposure setup and using SU-8 negative photoresist. Instead of using directly a glass slide to seal the chips, we sealed the devices by spin coating a thin layer of PDMS on 2"×3" microscope slides (Corning) and cured them partially until they were still tacky (about 12 minutes at 80°C) but wouldn't flow anymore. The final device was then assembled by placing the PDMS chip on top of the pre-cured PDMS thin film and was cured for another XXmin at 80°C. The fluids were delivered with high-precision syringe pumps (neMESYS, Cetoni) via PFA tubing (1/16" OD, 500 µm ID, IDEX Health Sciences).

The final chip design (see figure S1) consisted in a 75 µm high T-junction droplet generator with three water inlets and one oil inlet, all equipped with on-chip filter to prevent clogging due to dust/PDMS particles. The oil was introduced laterally via two symmetrical channels of 100 µm in width, and the three water inlets (90 µm in width) were joined directly at the junction (see Figure 1 in main text). The injection nozzle was 180 µm long and 50 µm wide, and led to a 150 µm wide accumulation channel.

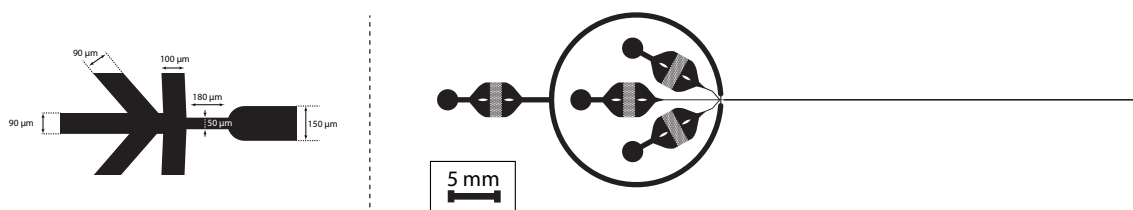


Figure S1. Details of the injection part of the chip (left) and complete illustration of the chip and its filters.

Reagents:

All the solvents and the reagents, including light mineral oil (Sigma-Aldrich), potassium tetracyanoplatinate (99.9%, Alfa Aesar), iron tetrafluoroborate (XX, supplier), pyrazine (99%, Sigma Aldrich), *n*-heptane (99%, Scharlau), ethanol (ACS reagent grade, Scharlau) and acetone (purissimum, Atlantic Labo) were used as received without additional purification.

Synthesis:

The high amount of pyrazine required for the reaction induces a significant change in the viscosity of the solutions which (for classical reaction conditions with 10 eq. of pyrazine in the solution containing the Fe(II) ions) causes a mismatch in the viscosity of the two reactant solutions (see Fig. S3), disturbing the operation of the chip. We therefore decided to use, for

the whole study, an equal partitioning of the pyrazine (10 eq.) in solutions A and B (i.e. 5 eq. in each solution).

1_{ref}: A 1 mL aqueous solution of K₂Pt(CN)₄ (99.3 mg, 0.23 mmol) was added dropwise to a 3.5 mL aqueous solution of Fe(BF₄)₂ (77.5 mg, 0.23 mmol) and pyrazine (18.4 mg, 0.23 mmol) under vigorous stirring at a rate of 300 μL/hour. The yellow product was filtered, washed with water and dried for 2 hours at 130°C.

1_{μF}: Two aqueous solutions (A and B) were prepared. K₂Pt(CN)₄ (138 mg, 0.32 mmol) and pyrazine (128 mg, 1.6 mmol) were dissolved in 2 mL of water (solution A) and Fe(BF₄)₂ (108 mg, 0.32 mmol) and pyrazine (128 mg, 1.6 mmol) were dissolved in 2 mL of water (solution B). The droplet microfluidic synthesis was performed by injecting the reactant solutions A and B together with an additional water stream W, and by generating droplets of reaction carried by a flow of mineral oil, with the following flow rates: Q_A = Q_B = 225 μL/h, Q_W = 450 μL/h and Q_{oil} = 3500 μL/h. The mixture was collected at the exit of the chip and most of the oil in the reaction mixture was removed through decantation. The solid yellow product was then washed three times by adding 15 ml of ethanol and centrifuging at 15000 RCF for 15 minutes, twice by adding 10 mL of *n*-heptane and centrifuging at 3000 RCF for 5 minutes, and once by adding 20 ml of acetone and centrifuging at 3000 RCF for 20 minutes. The resulting powder containing acetone was finally dried in vacuum at 100°C for 1h.

Characterizations:

TEM: Transmission Electron Microscopy (TEM) images were acquired on a JEOL JEM-1400 Plus at an acceleration voltage of 60 kV.

SEM: Scanning Electron Microscopy images were acquired on a JEOL JSM-6400.

Particle Size Distribution: Dynamic light scattering measurements were done on suspensions of micro-crystals in acetonitrile with a VASCO particle size analyzer from Cordouan Technologies, and are reported in number of particles. The size histograms were computed from TEM measurements on 272 particles for sample 1_{μF} and 138 particles for 1_{ref}.

FTIR: Fourier Transform Infrared spectra (FTIR) were measured on a Nicolet 6700 FTIR spectrometer in Attenuated Total Reflectance (ATR) mode.

Magnetic Susceptibility: Magnetic measurements were performed on a Microsense EZ7 Vibrating Sample Magnetometer with the 100-1000K EV1-LNA temperature control option. The sample were weighed accurately in a tin capsule, cold-sealed, and mounted on a 3 mm quartz rod with double-faced adhesive tape. DC measurements were performed under a 15 kOe magnetic field. A flow of nitrogen gas (12 standard cubic feet per hour) was used for temperature control. Background subtraction was performed using a closely matched empty tin capsule.

PXRD : powder X-ray diffraction analysis (PXRD) were performed on a PANalytical X'PERT MDP-PRO diffractometer (Cu-Kα radiation) equipped with a graphite monochromator using the θ-θ Bragg-Brentano geometry for sample 1_{ref} and a PANalytical X'PERT MDP-PRO diffractometer (Cu-Kα radiation) using the transmission capillary geometry equipped with a Goebel mirror for sample 1_{μF}. The samples were deposited on a silicon holder for Bragg-Brentano geometry and in a glass capillary for the transmission geometry.

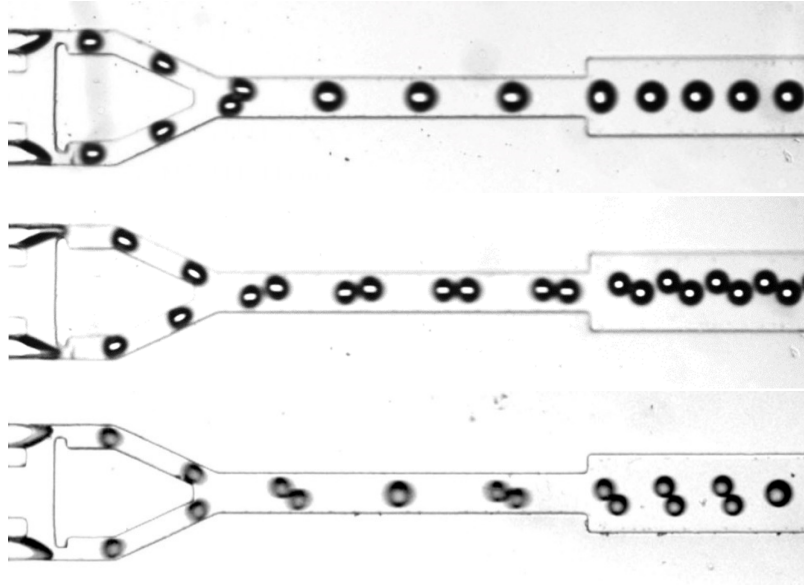


Figure S2. Optical microcopy images of droplet merging devices oscillating between merging and non-merging regimes due to imperfect coupling of the droplet pair generation.

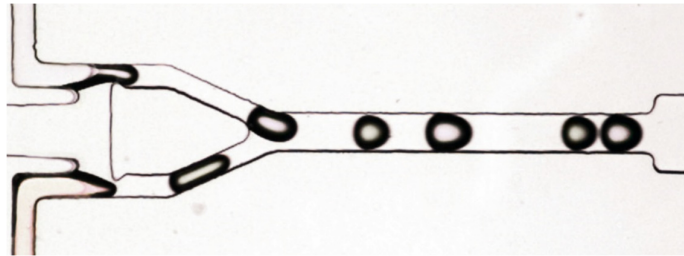


Figure S3. Optical microcopy images of a droplet-merging device showing the mismatch in droplet size and generation frequency due to the mismatch in viscosity caused by the excess of pyrazine in the solution introduced in the bottom channel.

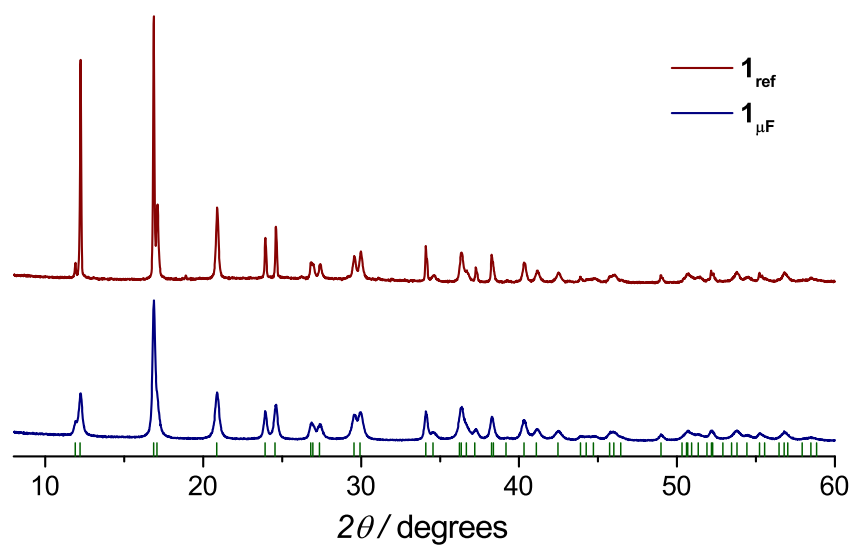


Figure S4. Comparison of the powder X-ray diffraction patterns for samples 1_{ref} (red) and $1_{\mu\text{F}}$ (blue). The green markers correspond to the expected Bragg peak positions (calculated from the reported structure).

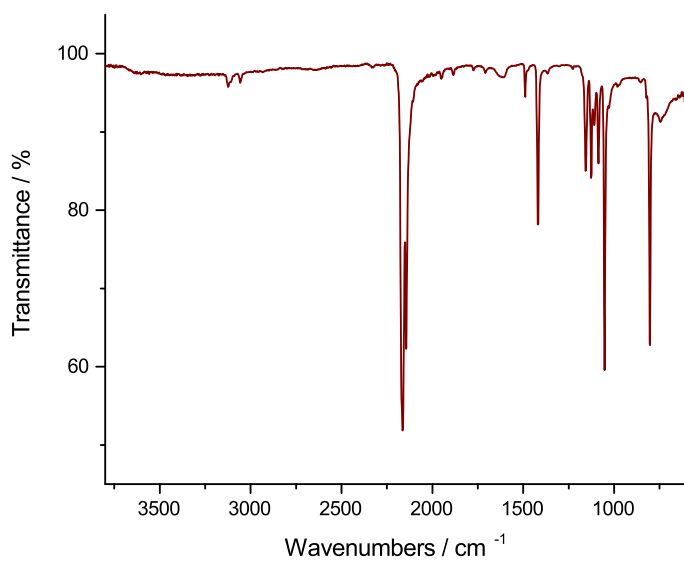


Figure S5. ATR-FTIR spectrum of **1_{ref}**.

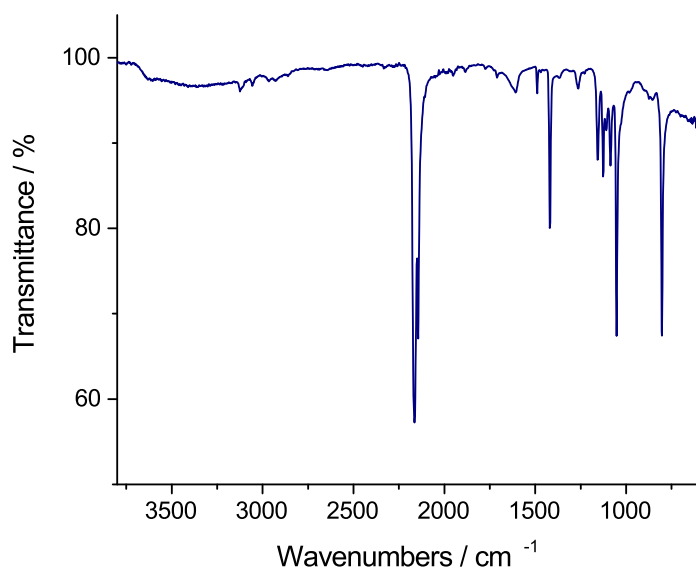


Figure S6. ATR-FTIR spectrum of **1_{uF}**.

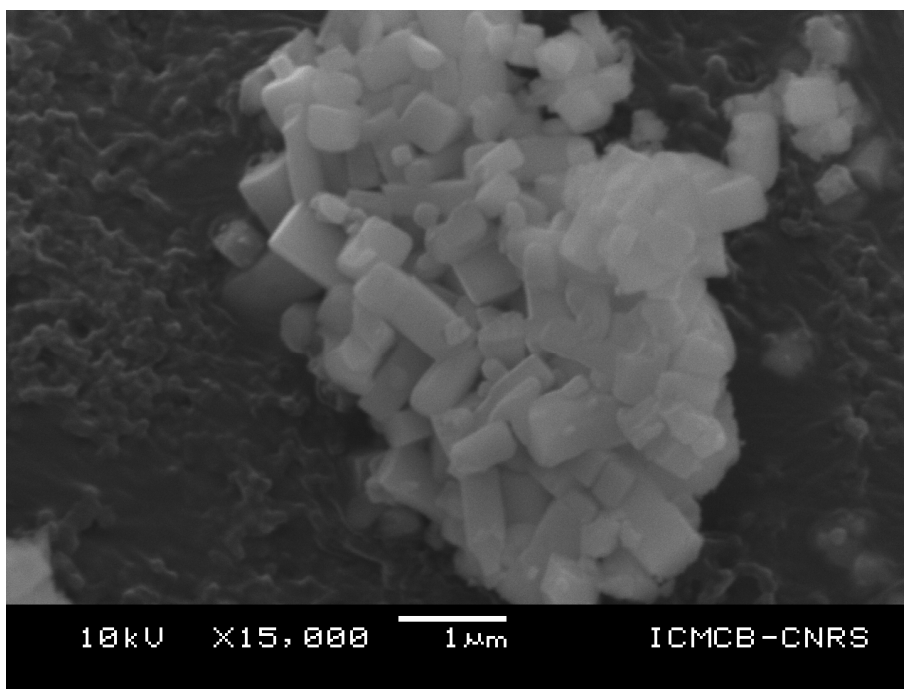


Figure S7. SEM image of 1_{ref} showing well resolved platelets.

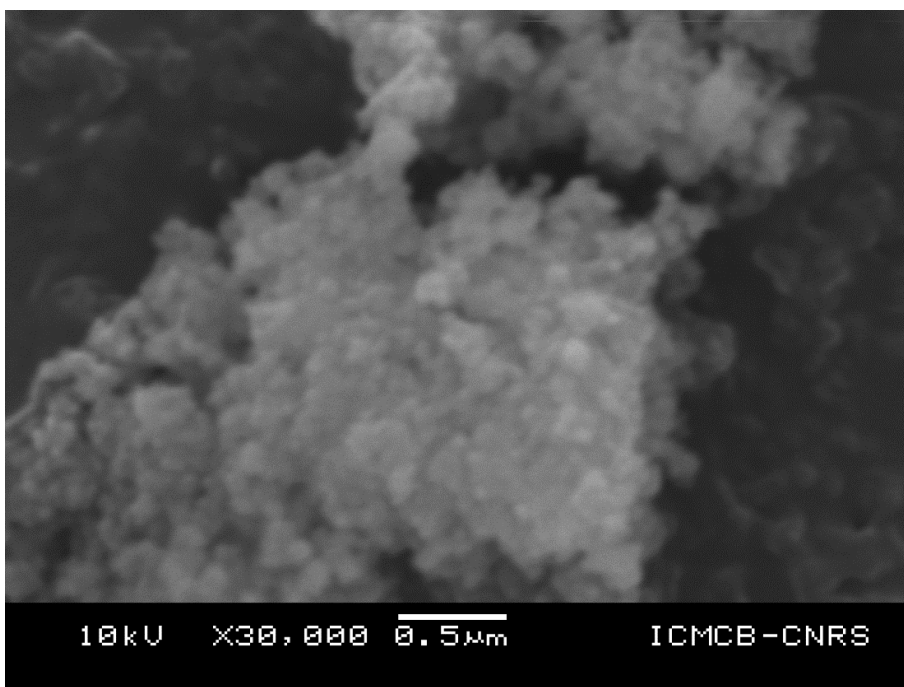
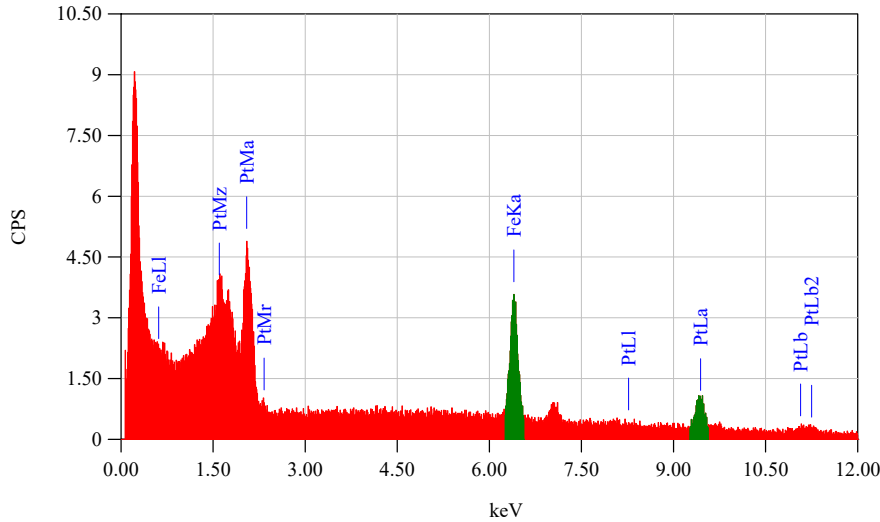


Figure S8. SEM image of $1_{\mu F}$. The nanocrystals are too small to be resolved, but it is clear that there are no crystals in the 1 µm range.



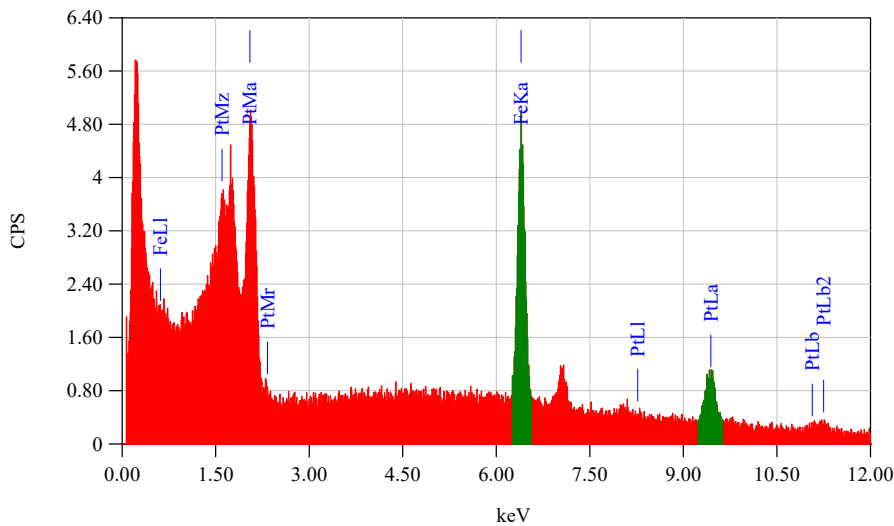
Acquisition Parameter
 Instrument : 6360(LA)
 Acc. Voltage : 15.0 kV
 Probe Current: 1.00000 nA
 PHA mode : T4
 Real Time : 160.57 sec
 Live Time : 123.31 sec
 Dead Time : 23 %
 Counting Rate: 1260 cps
 Energy Range : 0 - 20 keV

ZAF Method Standardless Quantitative Analysis

Fitting Coefficient : 0.2916

Element	(keV)	Mass%	Sigma	Atom%	Compound	Mass%	Cation	K
Fe K	6.398	22.42	0.39	50.23				28.4024
Pt L*	9.434	77.58	2.87	49.77				71.5976
Total		100.00		100.00				

Figure S9. EDS analysis of the Pt:Fe ratio for sample 1_{ref}.



Acquisition Parameter
 Instrument : 6360(LA)
 Acc. Voltage : 15.0 kV
 Probe Current: 1.00000 nA
 PHA mode : T4
 Real Time : 197.56 sec
 Live Time : 151.90 sec
 Dead Time : 23 %
 Counting Rate: 1264 cps
 Energy Range : 0 - 20 keV

PRZ Method Standardless Quantitative Analysis

Fitting Coefficient : 0.5138

Element	(keV)	Mass%	Sigma	Atom%	Compound	Mass%	Cation	K
Fe K	6.398	26.87	0.34	56.20				32.4570
Pt L*	9.434	73.13	6.31	43.80				67.6138
Total		100.00		100.00				

Figure S10. EDS analysis of the Pt:Fe ratio for sample 1_{μF}.

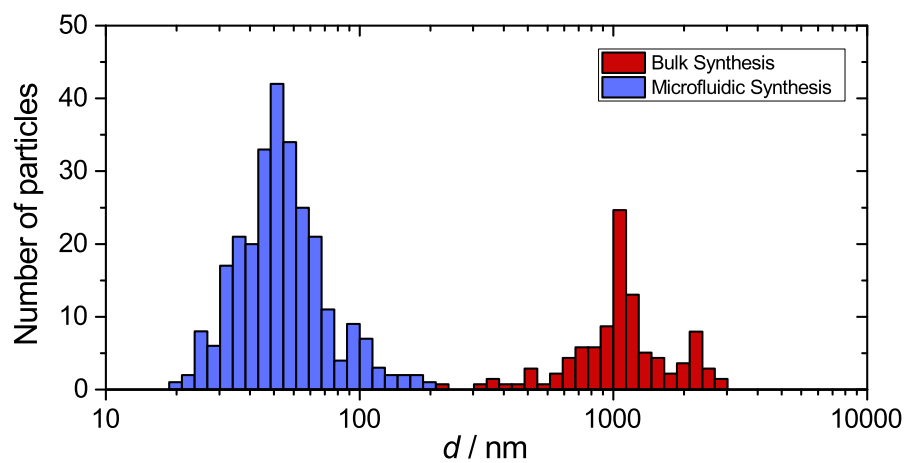


Figure S11. Size distribution in number of particles for the two samples.

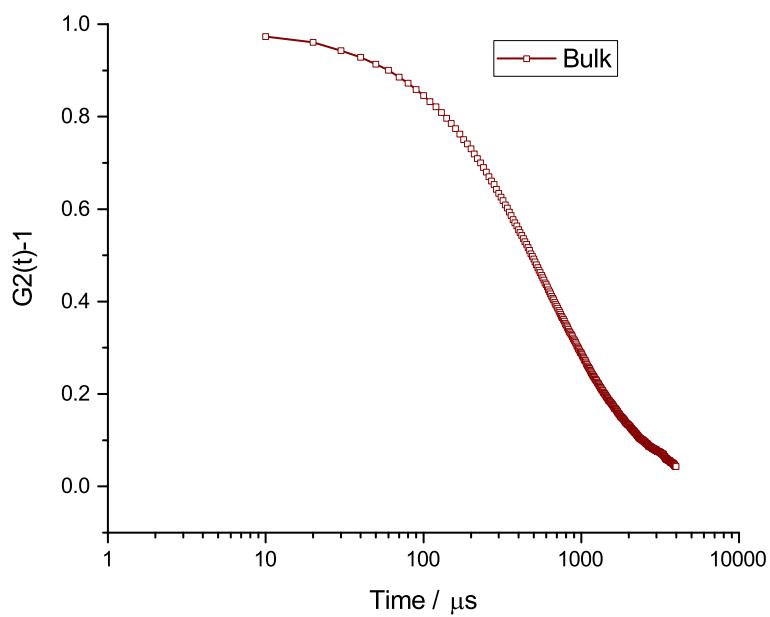


Figure S12. Experimental autocorrelation function for sample **1_{ref}**.

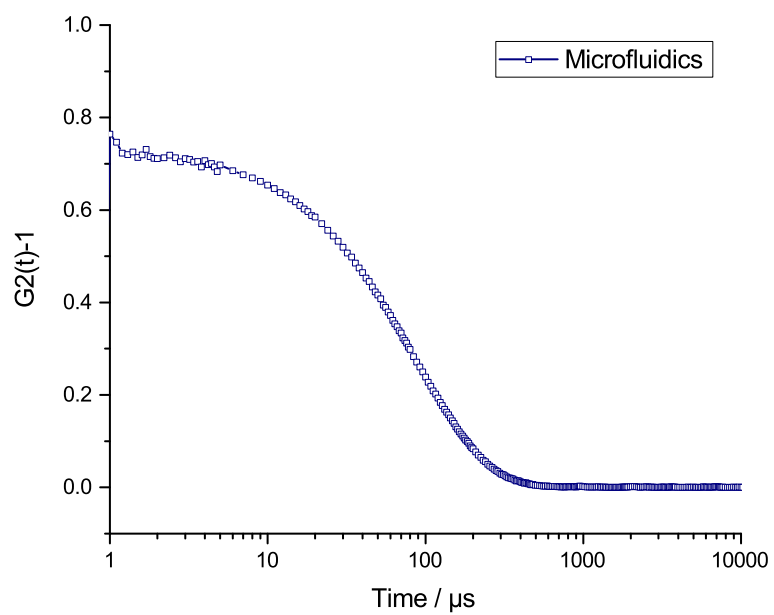


Figure S13. Experimental autocorrelation function for sample $1_{\mu F}$.

Analysis of the coherent domain size from the PXR measurements:

We performed whole powder pattern decomposition refinements according to the LeBail method¹ on the powder XRD patterns of both samples, which give mean values of the apparent coherent domain size as if it had a spherical shape. It is worth noting that these refinements provide an estimation of the coherent domain size, which is not necessarily related to the particle size in a direct manner. However, considering that a particle cannot be smaller than its coherent domain size, this analysis serves as a complementary and qualitative evidence of the particle downsizing effect presented in the main text.

Because of a strong effect of preferential orientation, the model we used for refinement is only a “profile matching” and not Rietveld. Therefore, nothing about atomic positions can be deduced from it. Moreover, using an isotropic model for the size broadening of the peaks some peaks appear wider than the model within specific directions, while others are narrower. This strongly suggest that an anisotropic size broadening model for the refinement (i.e. considering anisotropic domain dimensions) would provide a better estimate in good agreement with the final shape of the particles. Nevertheless, this goes beyond the scope of this paper and would likely require data of greater quality than the ones collected here. The refinements have been performed using the software JANA2006² using the fundamental parameter approach to extract the instrumental peak broadening.

Sample 1_{ref}:

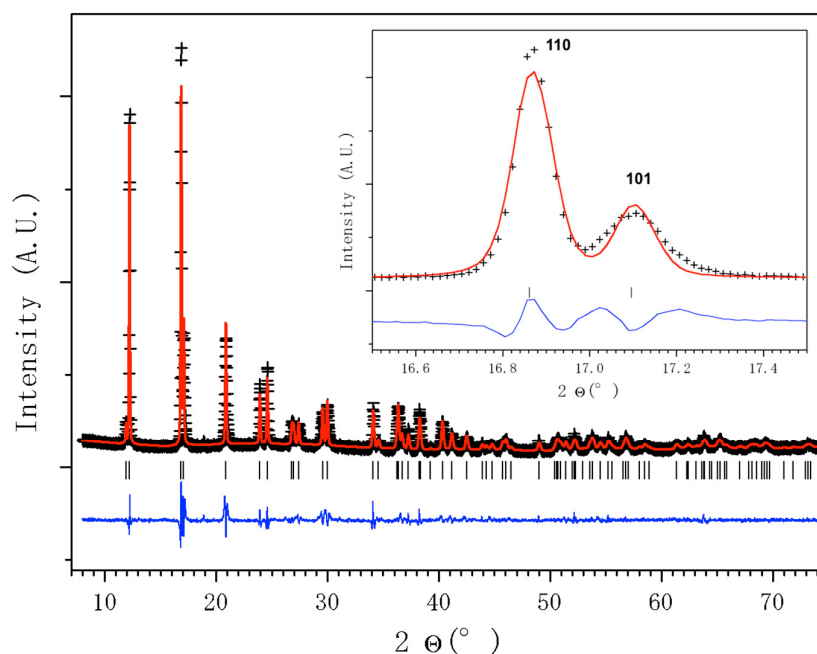


Figure S14. Profile matching refinement results for sample 1_{ref}. The black crosses correspond to the observed data; the red line, to the calculated one; the blue line, to the difference curve; and the black vertical lines, to the Bragg peak positions. Inset : anisotropic size broadening effect on 110 and 101 Bragg peaks (110 is narrower than the calculated peak and 101 is wider suggesting a platelets like shape)

This refinement leads to the following final parameters:

Unit cell parameters (a, b, c, α , β , γ , V ; Å, Å³)

7.4303(4) 7.4303(4) 7.2317(5) 90 90 90 399.3(1)

Reliability factors :

R_p = 4.73 ; R_{wp} = 7.01

Apparent size (volume weighted) : 176(12) nm.

Apparent strain : 21(1).10⁻⁴

Sample 1_{μF}:

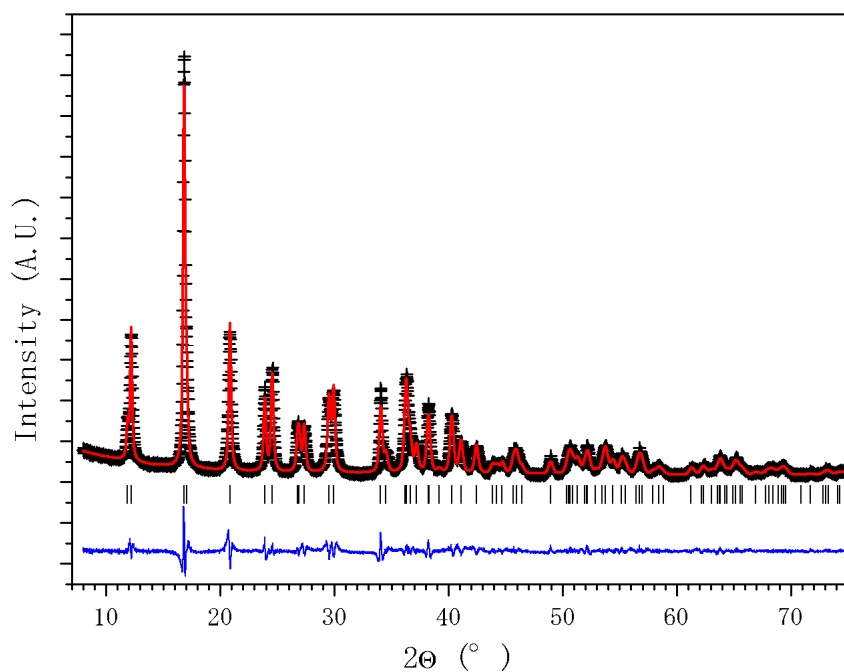


Figure S15. Profile matching refinement results for sample 1_{μF}. The black crosses correspond to the observed data; the red line, to the calculated one; the blue line, to the difference curve; and the black vertical lines, to the Bragg peak positions.

This refinement leads to the following final parameters:

Unit cell parameters (a, b, c, α , β , γ , V ; Å, Å³)

7.4397(15) 7.4397(15) 7.2460(20) 90 90 90 401.1(2)

Reliability factors:

R_p = 6.84 ; R_{wp} = 9.28

Apparent size (volume weighted): 34(1) nm.

Apparent strain: 30(2).10⁻⁴

1. A. Le Bail, *Powder Diffr.* **2005**, *20*, 316–326.
2. V. Petříček, M. Dušek, L. Palatinus, *Zeitschrift für Krist. - Cryst. Mater.* **2014**, *229*, 345–352.